Bulletin of the Seismological Society of America, Vol. 93, No. 5, pp. 1890–1903, October 2003

Performance of the Radial Semblance Method for the Location of Very Long Period Volcanic Signals

by Javier Almendros and Bernard Chouet

Abstract We investigate the performance of a source location method that combines multichannel semblance and particle motions and is being increasingly used to obtain estimates of the source locations of very long period (VLP) seismic signals recorded on volcanoes. The method makes use of the radial particle motions and large wavelengths that characterize the VLP events. To assess the capabilities of this radial semblance method, and to better understand its limitations, we quantify the effects of window length, noise contents of the signal, inaccurate velocity models, receiver coverage, and orientation errors in the horizontal components of the receivers. Our results show that the semblance method performs best when (1) the noise level is low enough to allow a good characterization of the waveforms, (2) the sources are located at distances between one half of the average receiver spacing and about two times the network aperture, and (3) the orientations of the horizontal components of the seismometers are known with relative accuracy. When these requirements are met, the radial semblance method constitutes an adequate tool to obtain preliminary locations of VLP volcanic signals recorded by broadband networks. Moreover, we provide a formula to determine the radial semblance level that should be used to define error regions associated to the estimated source locations.

Introduction

Volcanoes generate seismic energy at frequencies extending from zero (static displacements) to a few tens of hertz. Traditionally, different instruments have been used to record volcanic signals within different frequency ranges, namely dilatometers for quasi-static motions (e.g., Linde *et al.*, 1993) or short-period seismometers for signals in the 1- to 50-Hz range (e.g., McNutt, 1996). In the past decade, the use of broadband seismometers has allowed an extension of seismic measurements over the band 0.01–50 Hz, providing new and more complete insights into volcanic processes (Aster *et al.*, 2000).

In particular, strong interest has arisen in the detection and analysis of very long period (VLP) volcanic signals with dominant periods in the range of a few tens of seconds (Chouet, 1996). VLP signals have been observed at many volcanoes around the world, including Aso (Kaneshima *et al.*, 1996; Kawakatsu *et al.*, 2000; Legrand *et al.*, 2000), Miyake (Kumagai *et al.*, 2001), and Iwate (Nishimura *et al.*, 2000) in Japan; Merapi (Hidayat *et al.*, 2000, 2002) in Indonesia; Stromboli (Dreier *et al.*, 1994; Neuberg *et al.*, 1994; Chouet *et al.*, 1999, 2003) in Italy; Long Valley (Hill *et al.*, 2002) and Kilauea (Dawson *et al.*, 1998; Ohminato *et al.*, 1998; Almendros *et al.*, 2002a) in the United States; Popocatepetl (Arciniega-Ceballos *et al.*, 1999) in Mexico; and Erebus (Rowe *et al.*, 1998) in Antarctica. Common characteristics among these VLP signals are the simplicity of the waveforms, the radial, nearly rectilinear particle motions, and rapid decay of signal amplitude with distance from the source. VLP signals are intimately linked to the dynamics of a volcano and are commonly interpreted as representing a release of seismic energy in response to perturbations in the flow of magma and/or gas within volcanic conduits. Since their source is located within volcanic conduits, moment tensor inversions of VLP signals can provide reliable information on the geometry of magma plumbing systems beneath volcanoes, an important issue in the assessment of volcanic hazards. Moment tensor inversions of these signals also yield quantitative information about the dynamics of the magma transport (Uhira and Takeo, 1994; Ohminato *et al.*, 1998; Legrand *et al.*, 2000; Nishimura *et al.*, 2000; Chouet *et al.*, 2003). However, moment tensor inversions are usually time consuming, and the use of a preliminary method to approximately determine the source location becomes necessary.

In this article, we assess the performance of the radial semblance method, first applied by Kawakatsu *et al.* (2000) to the source location of VLP events recorded at Aso Volcano, Japan. This method combines information from multichannel semblance and particle motion and turns out to be especially useful for the location of the source of VLP volcanic signals.

Source Location Method

Most methods aimed at the location of seismic sources are related, in one way or another, to a determination of delays between wave arrivals at individual seismic receivers and inversion of these delays within the limits of a predefined velocity model. In the classic approach we determine the arrival times at each receiver of a seismic network for one or more of the seismic phases that can be identified in the seismograms, either by visual inspection or automated phase picking. These arrival times are then inverted within a particular velocity model, usually in the form of a layered half-space, to determine the source location and origin time. Although successful in its applications to tectonic earthquakes, this method suffers from severe limitations in the field of volcano seismology. Many seismic signals recorded on volcanoes are noisy and emergent, which makes the determination of reliable arrival times difficult or impossible. The resulting source location estimates have such large errors that in practice they may be useless.

Another approach to the source location problem is the determination of time delays between the signals recorded at different receivers based on a comparison of the corresponding waveforms. This method does not rely on the identification of any particular phase and therefore may be applied to any kind of signal, including small volcanic earthquakes and volcanic tremor. This approach works well when coherent signals are recorded at different receivers, enabling the determination of accurate delays. Due to path and site effects and the presence of noise, coherence among signals deteriorates with increasing receiver separation. Depending on the heterogeneity of the medium, we may not observe any similarities among waveforms recorded at receivers separated by distances exceeding a few wavelengths. The spatial decay of coherence is rapid for high-frequency signals. Quantitative analyses of the wave propagation properties of signals with frequencies in the range of a few hertz usually require the use of dense, small-aperture seismic antennas (Goldstein and Chouet, 1994; Chouet, 1996; Chouet *et al.*, 1997; Del Pezzo *et al.*, 1997; Almendros *et al.*, 1999, 2001b; Saccorotti *et al.*, 2001; Almendros *et al.*, 2002b). For periods in the VLP band, however, the wavelengths range from tens to hundreds of kilometers; hence, the signal coherence among receivers separated by a few kilometers is assured. The large wavelengths also facilitate the analysis because the effect of small-scale velocity heterogeneities is negligible and we may assume as a first-order approximation that the medium is homogeneous.

The source location method we investigate in this article relies on calculations of semblance and particle motions, and it is specifically designed for the location of isotropic sources using three-component seismometers (Kawakatsu *et al.*, 2000). The method determines the point for which the radial components of the signals recorded at different receivers, aligned to correct for the wave propagation delay, show maximum similarity. There are two implicit choices underlying this procedure, namely the selection of a magnitude to evaluate the similarity among waveforms and the choice of a velocity model for the medium, from which propagation delays can be estimated. Several methods are available to evaluate waveform similarity, including cross-correlation (Del Pezzo *et al.*, 1997; Almendros *et al.*, 1999), coherence (Ito, 1985; Poupinet *et al.*, 1996), and semblance (Neidel and Tarner, 1971; Kawakatsu *et al.*, 2000). We select semblance because it allows the inclusion of a penalty function to account for deviations of the particle motions from rectilinearity. The dependence of semblance locations on the velocity model used to represent the medium is discussed in detail later in the article.

Semblance

Semblance, as first introduced by Neidel and Tarner (1971), is a measure of the similarity of multichannel data defined as

$$S_0 = \frac{\sum_{j=1}^{M}\left(\sum_{i=1}^{N} U_i(\tau_i + j\Delta t)\right)^2}{N\sum_{j=1}^{M}\sum_{i=1}^{N} U_i(\tau_i + j\Delta t)^2}, \quad (1)$$

where Δt is the sampling interval, τ_i is the origin time of the window sampling the ith channel, $U_i(\tau_i + j\Delta t)$ is the jth time sample of the signal U recorded on the ith channel, and M and N represent the number of samples in the window and number of channels, respectively. S_0 is a number between 0 and 1, restrictive in the sense that 1 is only reached when the signals are identical, not only in waveform but also in amplitude. If we are interested only in the similarity among waveforms regardless of the amplitude, we need to use a new definition of semblance in which the signals U_i are normalized by their respective root mean square (rms). The new semblance is expressed as

$$S_0' = \frac{\sum_{j=1}^{M}\left(\sum_{i=1}^{N} \frac{U_i(\tau_i + j\Delta t)}{\sigma_i}\right)^2}{N\sum_{j=1}^{M}\sum_{i=1}^{N} \frac{U_i(\tau_i + j\Delta t)^2}{\sigma_i^2}} = \frac{1}{MN^2}\sum_{j=1}^{M}\left(\sum_{i=1}^{N} \frac{U_i(\tau_i + j\Delta t)}{\sigma_i}\right)^2, \quad (2)$$

where $\sigma_i = \sqrt{\frac{1}{M}\sum_{j=1}^{M} U_i(\tau_i + j\Delta t)^2}$ is the rms of the signal within the selected time window sampling the ith channel. This definition of semblance is equivalent to an averaging of the correlation coefficients of all possible channel pairs:

$$
\begin{aligned}
S_0' &= \frac{1}{MN^2}\sum_{j=1}^{M}\left(\sum_{i=1}^{N}\frac{U_i(\tau_i + j\Delta t)}{\sigma_i}\right)^2 \\
&= \frac{1}{MN^2}\sum_{j=1}^{M}\sum_{i=1}^{N}\frac{U_i(\tau_i + j\Delta t)}{\sigma_i}\sum_{k=1}^{N}\frac{U_k(\tau_k + j\Delta t)}{\sigma_k} \\
&= \frac{1}{N^2}\sum_{i,k=1}^{N}\frac{\sum_{j=1}^{M} U_i(\tau_i + j\Delta t)\, U_k(\tau_k + j\Delta t)}{M\,\sigma_i\sigma_k} \\
&= \frac{1}{N^2}\sum_{i,k=1}^{N}\frac{c_{ik}}{\sqrt{c_{ii}c_{kk}}},
\end{aligned}
\tag{3}
$$

where c_{ik} is the cross-correlation coefficient defined by

$$
c_{ik} = \sum_{j=1}^{M} U_i(\tau_i + j\Delta t)U_k(\tau_k + j\Delta t). \tag{4}
$$

To illustrate the difference between the definitions of S_0 and S_0', let us compare the semblance calculated for N records consisting of the same waveform delayed by τ_i, but with different amplitudes of the form $U_i(t) = A_i f(t - \tau_i)$. The first definition yields

$$
S_0 = \frac{\left(\sum_{i=1}^{N} A_i\right)^2}{N\sum_{i=1}^{N} A_i^2}, \tag{5}
$$

representing a number smaller than 1. In contrast, the second definition yields exactly $S_0' \equiv 1$. For example, the first definition is useful when comparing the performances of sensors with theoretically identical characteristics recording the same signal because, in principle, outputs should have identical waveforms and amplitudes. However, our purpose is to quantify the similarity among waveforms for a signal recorded at different receivers of a seismic network. The amplitude of the signal varies across the network, due in part to the geometrical spreading of the waves moving away from the source. As long as the waveforms remain approximately the same across the network, we do not want the signal amplitudes to affect the calculated semblance. Therefore, the use of the second definition is more appropriate.

Kawakatsu *et al.* (2000) introduced a modified definition of semblance to take advantage of three-component data. In this definition, practical for isotropic sources or windows containing *P*-wave motions, Kawakatsu *et al.* (2000) used the radial component of ground motion to compute semblance and introduced a penalty function to enhance the weight of receivers for which highly rectilinear particle motions are observed. The definition of semblance used by Kawakatsu *et al.* (2000), which we will refer to as radial semblance, is

$$
S_{\mathrm{iso}} = \frac{\sum_{j=1}^{M}\left(\left(\sum_{i=1}^{N} U_i^p(\tau_i + j\Delta t)\right)^2 - N\sum_{i=1}^{N}\left(U_i^v(\tau_i + j\Delta t)^2 + U_i^h(\tau_i + j\Delta t)^2\right)\right)}{N\sum_{j=1}^{M}\sum_{i=1}^{N}\left(U_i^p(\tau_i + j\Delta t)^2 + U_i^v(\tau_i + j\Delta t)^2 + U_i^h(\tau_i + j\Delta t)^2\right)} \tag{6}
$$

where the superscript p represents the component of ground motion, $\vec{U}_i$, in the source-receiver direction, and v and h represent two mutually perpendicular directions contained in the plane perpendicular to the p direction. As done before, we avoid the effect of the relative amplitudes of the signals by normalizing each component by the rms of the three-component data, defined as

$$
\sigma_i = \sqrt{\frac{1}{M}\sum_{j=1}^{M} |\vec{U}_i(\tau_i + j\Delta t)|^2}. \tag{7}
$$

Accordingly, a new expression for radial semblance is obtained as

$$
\begin{aligned}
S_{\mathrm{iso}}' &= \frac{1}{MN^2}\sum_{j=1}^{M}\left(\left(\sum_{i=1}^{N}\frac{U_i^p(\tau_i + j\Delta t)}{\sigma_i}\right)^2 - N\sum_{i=1}^{N}\left(\frac{U_i^v(\tau_i + j\Delta t)^2}{\sigma_i^2} + \frac{U_i^h(\tau_i + j\Delta t)^2}{\sigma_i^2}\right)\right) \\
&= \frac{1}{MN^2}\sum_{j=1}^{M}\left(\left(\sum_{i=1}^{N}\frac{U_i^p(\tau_i + j\Delta t)}{\sigma_i}\right)^2 + N\sum_{i=1}^{N}\left(\frac{U_i^p(\tau_i + j\Delta t)}{\sigma_i}\right)^2\right) - 1,
\end{aligned}
\tag{8}
$$

which yields a number between -1 and 1. In this article, we scale S_{iso}' to the range between 0 and 1 and use the following definition of radial semblance:

$$
\begin{aligned}
S &= \frac{S_{\mathrm{iso}}' + 1}{2} \\
&= \frac{1}{2MN^2}\sum_{j=1}^{M}\left(\left(\sum_{i=1}^{N}\frac{U_i^p(\tau_i + j\Delta t)}{\sigma_i}\right)^2 + N\sum_{i=1}^{N}\left(\frac{U_i^p(\tau_i + j\Delta t)}{\sigma_i}\right)^2\right).
\end{aligned}
\tag{9}
$$

Location Procedure

The application of the semblance method consists in finding a set of arrival times $\{\tau_i,\ i = 1 \ldots N\}$ that yields a maximum radial semblance for the N-channel data. For a

particular source location, the arrival times can be expressed as

$$\tau_i(\vec{r}) = t_0 + \tau_i'(\vec{r}), \tag{10}$$

where t_0 is the event origin time and τ_i' is the travel time from the source to the ith receiver. The travel times depend on the assumed source position and on the velocity model used to represent the medium. For example, if we select a homogeneous medium with velocity v, the travel times are given by

$$\tau_i'(\vec{r}) = \frac{|\vec{r} - \vec{r}_i|}{v}, \tag{11}$$

where $\vec{r}$ represents the source location and $\vec{r}_i$ is the location of the ith receiver.

The procedure used to obtain a source location by the semblance method consists of the following steps. We first determine the spatial extent of the region of interest by defining a three-dimensional grid of assumed source positions, broad enough to include the actual source. Travel times are computed from every node of the grid to every receiver of the network using equation (11). We then fix the interval of signal considered by selecting the start time t_w of the analysis window having duration $M\Delta t$. This selection effectively implies that for each grid node the origin time is

$$t_0(\vec{r}) = t_w - \min(\tau_i'(\vec{r})). \tag{12}$$

Finally, we apply equation (9), in which we use the arrival times calculated for each node of the source grid. In this way, we obtain a three-dimensional distribution of radial semblance, $S(\vec{r})$.

We repeat the procedure by sliding the analysis window by a fixed increment along the signal. This yields a series of spatial distributions of radial semblance. To obtain a unique solution and to enhance the stability of the location, we average the radial semblance distributions corresponding to those windows within which the maximum radial semblance is higher than 90% of the absolute maximum obtained for all the windows. Two kinds of information are contained in the average radial semblance distribution. On the one hand, the point at which the radial semblance reaches its maximum can be regarded as the most likely source position for the analyzed signal. On the other hand, the shape of the maximum, that is the rate at which radial semblance decays as we move away from the maximum value, provides some idea of the resolution of the solution.

Performance of the Semblance Method

Several authors have applied the semblance method to the location of VLP signals in volcanoes (Furumoto *et al.*, 1992; Chouet and Dawson, 1997; Ohminato *et al.*, 1998; Chouet *et al.*, 1999; Kawakatsu *et al.*, 2000; Nishimura *et al.*, 2000; Almendros *et al.*, 2002a). The basic assumption underlying this approach is that the spatial maximum of the semblance distribution yields the most likely source location. An error in source position is defined as the size of the region within which semblance is above a certain level. As there is no straightforward approach to define this level, it is usually fixed *a priori* to some percentage of the maximum semblance.

In the following, we perform a series of synthetic tests to better understand the capabilities and limitations of the semblance method. These tests assess the effects of window length, noise contents of the signal, receiver coverage, misorientations of horizontal components, and inaccurate velocity models.

Synthetic Environment

We analyze the performance of the semblance method with synthetic seismograms generated for a circular network with an aperture of 4 km (Fig. 1). The network features nine three-component receivers embedded in an infinite homogeneous medium with constant velocity $v = 4$ km/sec. We consider an isotropic source with source time function given by

$$u(t) = A\left(\frac{t}{t_0}\right)^n \exp(-t/t_0)\,\sin(2\pi f t), \tag{13}$$

with $A = 0.22\,\mu$m/sec, $n = 4$, $t_0 = 6$ sec, and $f = 0.05$ Hz. The sampling interval is 0.2 sec. The source signal has a spindle-shaped envelope with maximum amplitude of 1 μm/sec, and it consists of a few monochromatic oscillations with period of 20 sec lasting ~60 sec (see Fig. 2). These features mimic the VLP signals observed at Kilauea Volcano, Hawaii (Dawson *et al.*, 1998; Ohminato *et al.*, 1998; Almendros *et al.*, 2002a). Assuming radial propagation away from an isotropic source, we may express the three-component seismograms as

$$U_i^k(t) = \begin{cases} n^k(t) & t < \tau_i \\ u(t - \tau_i)\,\dfrac{r^k - r_i^k}{|\vec{r} - \vec{r}_i|}\,\dfrac{D^2}{|\vec{r} - \vec{r}_i|^2} + n^k(t) & t \geq \tau_i \end{cases}, \tag{14}$$

where $k = 1, 2, 3$ is an index representing the east, north, and vertical directions, respectively; $\vec{r}$ and $\vec{r}_i$ are the positions of the source and ith receiver in the network; $D = \min(|\vec{r} - \vec{r}_i|, i = 1 \ldots N)$ is the distance between the source and the closest receiver; and $\vec{n}(t)$ represents the contribution of random noise. Note that the seismograms are normalized so that the signal amplitude at the closest receiver is 1 μm/sec. We assume a geometrical spreading factor of r^{-2}. The full solution for the wave field generated by an isotropic source includes another term with r^{-1} dependence (e.g., Aki and Richards, 1980). However, in light of the large wavelengths involved, the near-field term clearly

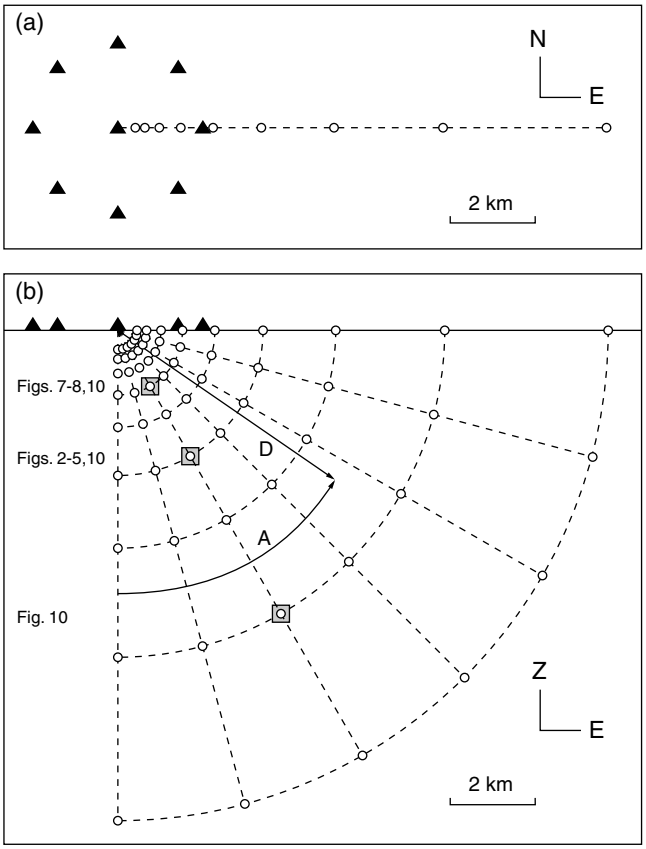

Figure 1. Configuration of the network (triangles) and source locations (open circles) used to generate the synthetic signals analyzed in this article. (a) Map view. (b) East–west vertical cross section. The position of each source is determined by the polar coordinates, D (distance from the center of the network) and A (angle between the vertical and network hub-to-source direction). The circles overlying the gray squares mark the source locations used to generate the figures indicated at the left.

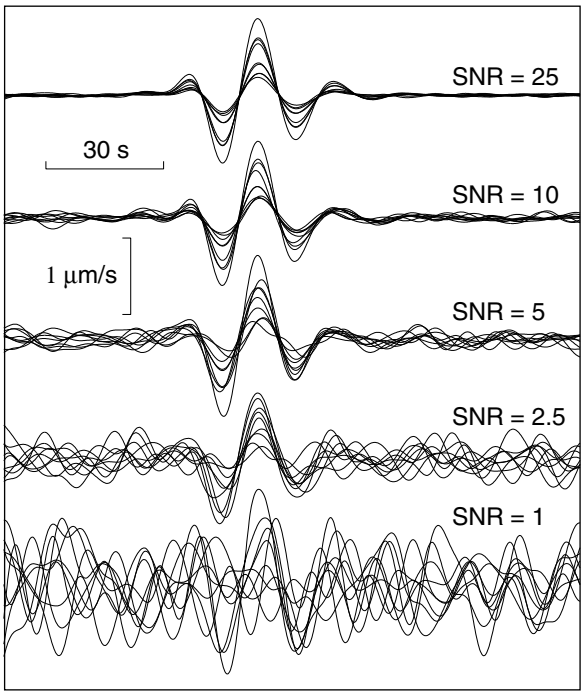

Figure 2. Examples of synthetic vertical-component seismograms generated for different SNRs. The source is located at $D = 3.4$ km and $A = 30°$ (see Fig. 1). The nine waveforms corresponding to the nine receivers of the network are overlain for each SNR.

dominates the radiation up to distances of 10 km. We simulate the noise in the VLP band by using independent Gaussian time series filtered in the 5- to 50-sec band for each component. Although VLP noise has not been studied in depth, we have observed that (1) the particle motions show no particular polarization and (2) semblance calculated for pure VLP noise produces very low values, below 0.4. This lack of coherence among waveforms with very long wavelengths recorded at stations just a few kilometers apart strongly suggests that noise mostly originates at the sensor in the form of thermal and electronic noise. Therefore, we feel that our pink noise model is appropriate to simulate the noise within the context of the present study.

Effect of Window Length

To assess the effect of window length we consider windows with lengths of 5, 10, 20, 30, and 50 sec applied to synthetic seismograms from a source located at a distance of 3.4 km along a line oriented 30° from the vertical (see Fig. 1). Our results indicate that short windows yield higher values of maximum semblance but induce more variability in source location from window to window along the signal because particle motion directions are not well defined when considering just a fraction of the signal period. Long windows yield smaller values of semblance because such windows include a greater amount of noise; however, the source locations are more stable. The selection of a window length must accommodate this trade-off between maximum semblance and stability. Based on our experience with real signals, we conclude that a window length containing between one and two cycles of the dominant period provides the best performance. In the following analyses, we select a window length of 30 sec and a sliding increment of 10 sec.

Effect of Noise Contributions at Different Epicentral Distances and Depths

We test the location capabilities of our synthetic network for a set of sources located at different epicentral distances and depths. For each source, the accuracy of the locations obtained by the semblance method depends on the level of noise. We use the symmetry of the problem and restrict our calculations to positive values of the east coordinate and negative values of the vertical coordinate within the east–west vertical plane passing through the center of the

network. We define a grid of sources in polar coordinates (Fig. 1b). In this grid, sources are positioned at distances D from the center of the network, with $D = 450 \times 1.5^j$ m, $j = 0, \ldots, 8$, along lines inclined by an angle A from the vertical, with $A = 15k°$, $k = 0, \ldots, 6$. For each of the 63 point sources considered, we investigate the effects of different noise contributions by generating noisy three-component seismograms at each receiver (equation 14). The amount of noise is characterized by a network-averaged signal-to-noise ratio (SNR) defined as

$$\text{SNR} = \frac{1}{N}\sum_{i=1}^{N}\frac{\max|\vec{U}_i| - \sigma_i^n}{\sigma_i^n}, \qquad (15)$$

where $|\vec{U}_i|$ is the modulus of the velocity recorded at the ith receiver and σ_i^n represents the rms of the seismogram within a window containing only noise. For each source location, we generate noisy seismograms with average SNRs of 5, 2, 1, 0.5, and 0.2. Filtering the signals in the 5- to 50-sec band improves the SNR by a factor of 5. Therefore, the given values represent average SNRs in the 5- to 50-sec band of 25, 10, 5, 2.5, and 1. The 5- to 50-sec band represents the band most commonly selected in investigations of VLP signals in volcanoes. Figures 2 and 3 show examples of synthetic vertical-component signals at the nine receivers and their corresponding particle motions, respectively, obtained for the selected values of SNR.

For each source location and for each of the five values of SNR, we generate 25 independent sets of seismograms to provide a meaningful statistical ensemble and adequately represent the effect of noise on the source locations. We apply the semblance method to each set of seismograms and estimate the corresponding semblance distribution and source location as a function of the source position and SNR. The analyses are performed over domains centered on the source location. Each domain is discretized into $51 \times 51 \times 51$ nodes with a constant cell size, whose value is fixed based on the distance between the center of the network and the source (see Table 1). To characterize the solutions, we measure the following three parameters of the semblance distributions: (1) the average maximum semblance, $S_{\max}$, which provides information on the quality of the locations and indicates whether the waveforms and particle motions are consistent with a single point source or a diffuse source region; (2) the average difference between the maximum semblance and semblance at the actual source location, $\Delta S = S_{\max} -$

Table 1
Cell Size Used for the Semblance Locations

D (km)	0.5	0.7	1.0	1.5	2.3	3.4	5.1	7.7	11.5
Cell size (m)	15	20	30	50	80	100	200	300	400

The cell size is a function of the distance, D, from the center of the network to the source.

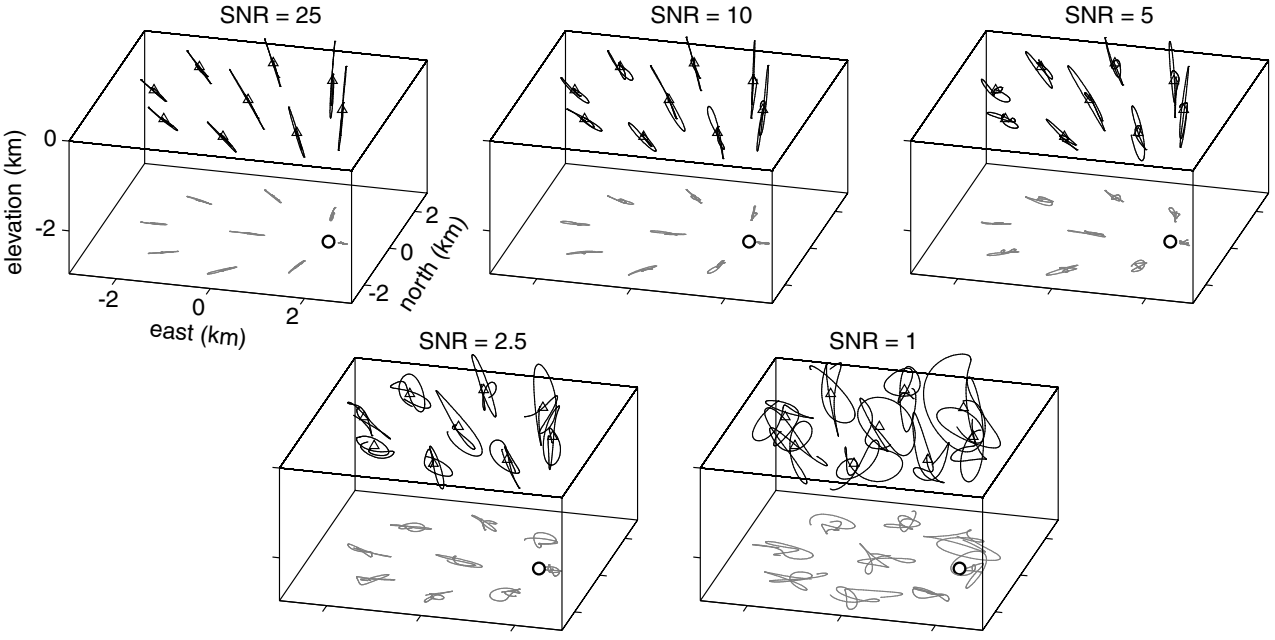

Figure 3. Three-dimensional views of the particle motions (black lines) of synthetics generated for different SNRs. The positions of the receivers are indicated by triangles on the top surface of each cube. An open circle marks the location of the source at $D = 3.4$ km and $A = 30°$. This source location is the same as that used to generate the seismograms shown in Figure 2. Horizontal projections of the particle motions (gray lines) are plotted on the bottom face of each cube, at the level of the source depth.

S_0, which yields the semblance level we need to consider when assessing location errors if we want these errors to include the source location; and (3) the average distance between the actual and estimated source locations, ΔD, which is an estimate of the magnitude of the expected location error.

The presence of noise reduces both the similarity between waveforms and the rectilinearity of the signals, thereby strongly decreasing the value of semblance estimated with equation (9). Rectilinearity is defined as $L = 1 - (\lambda_2/\lambda_1)$ (Montalbetti and Kanasewich, 1970), in which λ_1 and λ_2 are the first and second largest eigenvalues of the covariance matrix of the three components of motion. While rectilinearity reaches values near 1 for high SNRs, it may drop to less than 0.5 for an SNR of 1 (see particle motions in Fig. 3). It is worth noting here that the formulation of the problem with equation (9) implies an equivalency between the results obtained for signals containing random contributions from noise and signals with marked ellipticity, as long as the rectilinearities remain similar.

Figure 4 shows examples of source locations obtained for different SNRs for the source considered in Figures 2 and 3. The calculated source locations are distributed around the actual source location. The size of the cluster of solutions increases with the level of noise. For sources located within the network the clusters are usually spherical; however, for distant sources and low SNRs these clusters tend toward ellipsoidal shapes that are elongated along the network–source direction. In extreme situations the clusters become asymmetric due to the reduced resolution of the method with distance. The clusters exhibit smaller location errors when the estimated source locations are closer to the network than the actual source location and larger location errors when the estimated source locations are farther than the actual source location. In the latter cases, the clusters have the shapes of paraboloids rather than ellipsoids. The gray contours in Figure 4 correspond to a level of semblance equal to S_0, which is the value of semblance at the actual source location. These regions, within which semblance is higher than S_0, always contain the actual source location, a fact that will be used later to define location errors in the semblance method. For high SNRs, semblance decays rapidly with increasing distance from the location of the maximum semblance. In such cases, the S_0 contours define small volumes. For low SNRs, the peak of semblance is more rounded and the volumes contained within the S_0 contours become larger. For a SNR of 1, these regions are unbounded and a location error can not easily be assessed.

Figure 5 shows the values of $S_{\max}$, $\delta S = \Delta S/S_{\max}$, and $\delta D = \Delta D/D$ as functions of SNR for the semblance locations displayed in Figure 4. We observe that the quality of the source locations is strongly affected by the presence of noise. $S_{\max}$ ranges from ~ 1 for SNRs > 5 to less than 0.5 for SNR $= 1$ (Fig. 5a). The difference between the maximum semblance and the value of semblance at the actual source location increases from nearly 0 to more than 4% of the maximum semblance (Fig. 5b), and average location errors may range up to about 50% of the distance from the source to the center of the network (Fig. 5c). Semblance distributions for low SNRs are wider than for high SNRs, which should yield smaller values of δS since the variation of semblance with distance is smoother. Nevertheless, both the decrease of $S_{\max}$ and the increase of δD with increasing noise contents contribute to the net increase of δS with decreasing SNR. In any case, the large scatter of δS and δD for low SNRs suggests that small values of $S_{\max}$ should not be considered significant.

Figure 6 shows the average values of $S_{\max}$, δS, and δD for an SNR of 5 for sources positioned at the grid nodes (open circles) shown in Figure 1. We observe that the averages of $S_{\max}$, δS, and δD remain within the same approximate ranges for all source locations, except for two extreme cases. The first case represents distant sources for which the network subtends a small solid angle as viewed from the source, resulting in a poor definition of the crossing location of the particle motion directions. For such sources, the distances between receivers are also small compared to the distance from the network to the source, so that the differences between arrival times at the different receivers are small, in some cases smaller than the sampling rate. Our results point to a slight tendency to lower quality solutions for sources at increasing distances, as indicated by the increase of δD with distance in Figure 6. The second case represents sources that are located too close to one of the receivers. In this situation, seismograms at the remaining receivers contain comparatively little energy in accord with the r^{-2} spreading term used to generate the synthetic signals. The ratio of distance from the source to the closest receiver versus average distance from the source to the remaining receivers provides a measure of this effect. When this ratio is larger than ~ 3, the nearest seismogram contains a signal with an amplitude more than 10 times larger than the other seismograms, so that even a small amount of noise introduces large errors in the source location obtained by the semblance method. For example, for a source located at $D = 2.3$ km and $A = 90°$ (the position marked by an arrow in Fig. 6), the nearest receiver is only 0.3 km from the source, while the average distance to the other receivers is ~ 3.0 km. This translates into an amplitude ratio of more than 100, which explains the anomalous results obtained for this source location and general trend to produce lower quality solutions with decreasing distance (see Fig. 6). This problem might be solved simply by using a subset of the network from which the nearest station has been eliminated. However, this operation introduces a change in the configuration of the network (see the next section) and artificially reduces the average SNR of the signal, both of which have a negative effect on the location capabilities of the semblance method.

The spatial distributions of $S_{\max}$, δS, and δD obtained for other SNRs display features similar to those seen in Figure 6. In general, a lower SNR produces lower values of $S_{\max}$ and higher values of δS and δD for every source location

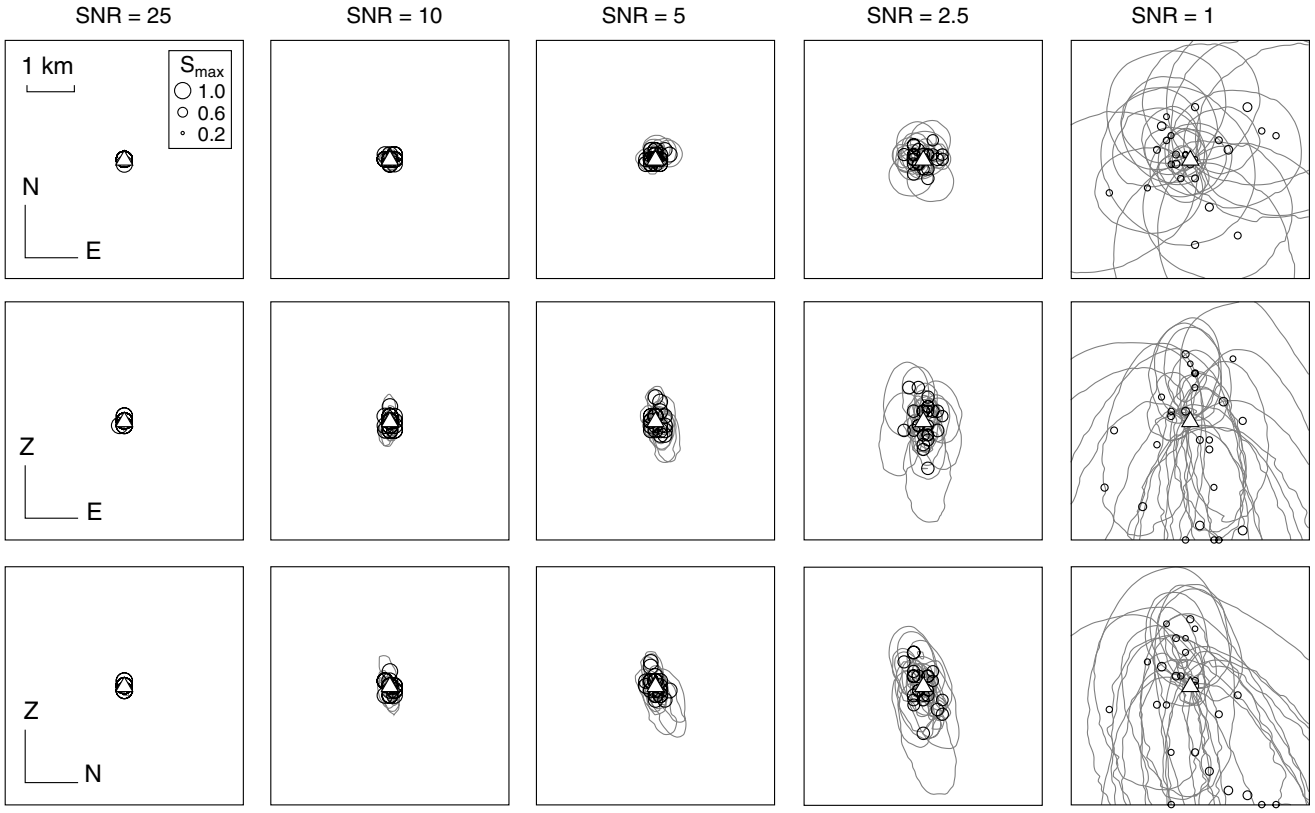

Figure 4. Results of 25 semblance locations performed on 25 sets of synthetic seismograms generated for a point source located at $D = 3.4$ km and $A = 30°$ (same source location as used in generating Figs. 2 and 3) and for different SNRs. Each row corresponds to a cross section through the actual source location and each column to a different SNR. The original source location is indicated by the white triangle at the center of each plot. Open circles represent projections on the cross sections of the source locations obtained by the semblance method. Circle sizes are proportional to the maximum semblance of the distributions (see scale in top left panel). The gray contours outline the intersections of the cross section with the volumes within which the calculated semblance is higher than the value of semblance at the actual source location. This value is selected in such a way that the source location is always contained within the gray contours (see text for details).

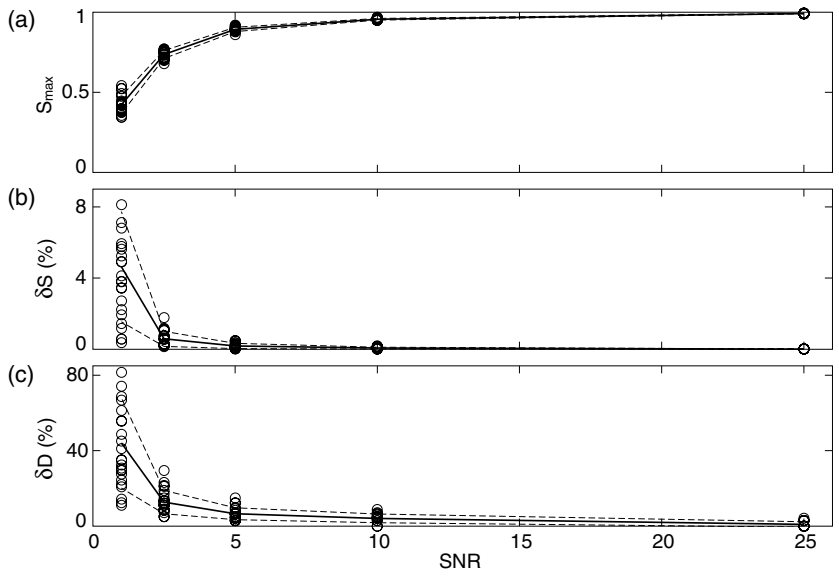

Figure 5. Variation of S_{max}, δS, and δD selected to characterize the semblance locations as a function of SNR for the solutions in Figure 4. (a) Maximum semblance, S_{max}, corresponding to the maximum of the semblance distribution. (b) Difference between the maximum semblance and the semblance at the source, expressed as a percentage of the maximum semblance, δS. (c) Distance between the actual and estimated source location, expressed as a percentage of the distance from the actual source to the center of the network, δD. The solid lines represent the average values, and dashed lines represent standard deviations.

considered, while high values of SNR have the opposite effect (for example, see Fig. 5). Comparing values obtained at different source locations, we find the same anomalous behavior for sources located close to one of the receivers or too far from the network. Therefore, the two situations described hold for any of the SNRs considered, although the absolute values of these anomalies tend to increase with decreasing SNR.

From these analyses we conclude that the semblance method is efficient when the average SNR of the seismograms is higher than about 2.5, and when the sources range in distances between roughly a half of the average receiver spacing and two times the network aperture. For sources located within this range, the results are relatively independent of the source position. The main factor governing the accuracy of the solution is the level of noise. The averages of the semblance parameters obtained for source locations within this range are given in Table 2 for the different SNRs considered.

Configuration of the Network

The ideal configuration of a seismic network, with complete azimuthal coverage of the source region of interest, may not always be achievable due to logistic challenges such as site remoteness, difficulty of access, or limitations in data transmission. Even when good coverage is achieved, some receivers may fail during some periods of time. To assess the effect of partial network coverage, we generate seismograms in the same way as in the previous section for two networks that include only the six receivers in the western half, or six receivers in the northern half of the original network, respectively. Figure 7 shows examples of the semblance locations obtained with the two reduced networks, compared to the locations obtained with the complete network. Our results indicate that semblance locations obtained with the reduced networks yield average S_{max} values that are similar, or even slightly higher, than the values obtained for the complete network (Table 2). However, we should not be misled by this result, which only reflects the ease with which one can obtain a good match of the waveforms and particle motions with a smaller number of signals. Values of δS and δD are twice as large compared to the values obtained with the complete network (see Table 2). Source locations tend to be biased in the directions where the partial networks lack receiver coverage as compared to the original network (compare Fig. 7b,c with Fig. 7a).

Errors in the Orientations of the Horizontal Components

A precise knowledge (within $\sim 1°$) of the orientations of the horizontal receiver components is generally difficult to achieve in the field. Accurate orientations are often determined *a posteriori*, for example by observation of the horizontal particle motions produced by teleseisms (Dawson *et al.*, 1998). It is therefore likely that small errors may exist that affect the directions of the particle motions and conse-

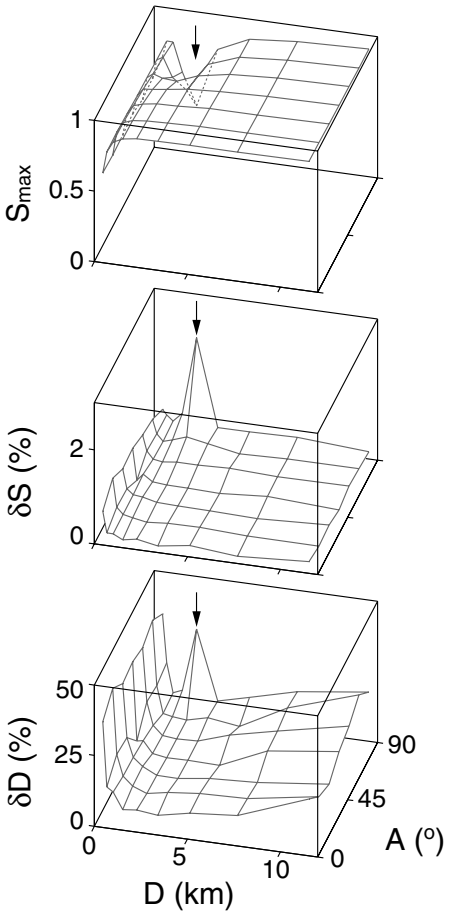

Figure 6. Spatial distributions of S_{max}, δS, and δD for an SNR of 5. The arrows point to the anomalous behavior of these parameters due to the close proximity of the source to one of the receivers (see text for explanations).

Table 2
Average Results Obtained from the Semblance Method for Different Values of SNR

	Noise Only			Orientation Errors		
SNR	S_{max}	δS(%)	δD(%)	S_{max}	δS(%)	δD(%)
25	0.98	0.01	1.5	0.96	0.05	6.5
10	0.94	0.06	5.8	0.93	0.16	8.8
5	0.85	0.23	10.9	0.85	0.36	13.9
2.5	0.67	0.81	21.4	0.68	1.00	23.0
1	0.40	3.93	47.4	0.40	3.95	49.6
	Western Half Network			Northern Half Network		
SNR	S_{max}	δS(%)	δD(%)	S_{max}	δS(%)	δD(%)
25	0.98	0.02	3.0	0.99	0.02	3.3
10	0.93	0.13	8.9	0.95	0.12	9.6
5	0.84	0.48	17.4	0.88	0.45	18.6
2.5	0.68	1.58	32.4	0.71	1.55	34.6
1	0.42	6.52	59.9	0.43	6.37	65.6

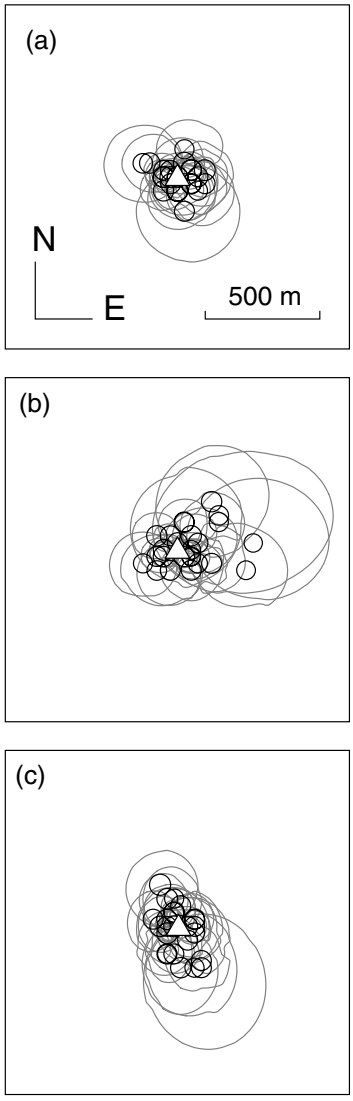

Figure 7. Comparison between semblance locations obtained from the analysis of 25 sets of seismograms generated for the complete network and two reduced networks discussed in the text. The source is located at $D = 1.0$ km and $A = 30°$, and the SNR is 5. (a) Semblance locations obtained with the complete network. (b) Semblance locations obtained with a reduced network consisting of the western half of the original network. (c) Semblance locations obtained with a reduced network consisting of the northern half of the original network.

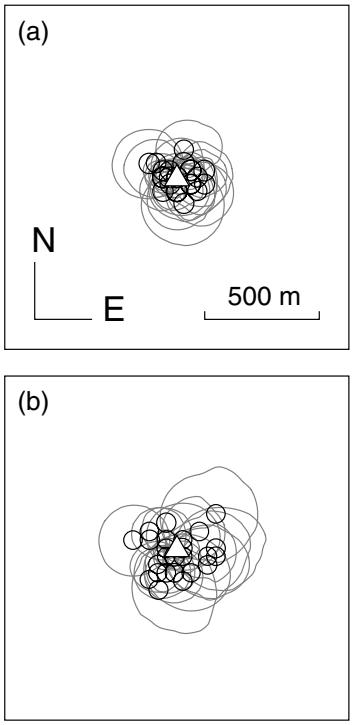

Figure 8. Comparison between semblance locations obtained from the analysis of 25 sets of seismograms generated for random orientation errors in the horizontal components of the receivers. The source is located at $D = 1.0$ km and $A = 30°$, and the SNR is 5. (a) Semblance locations performed with precise knowledge of the orientations of the horizontal components of the receivers (same as Fig. 7a). (b) Semblance locations including random errors within the range $\pm 10°$ in the orientations of the horizontal components of the receivers.

quently the semblance results. In this section, we test the effect of such errors by applying the semblance method to seismograms whose north–south and east–west components have been rotated a random angle, different at each receiver, within a range of $\pm 10°$.

Our results indicate that these misorientations may be an important source of errors, especially for shallow sources (Fig. 8). In this case, the semblance distributions are broader and yield values of S_{max} that are smaller than those obtained by including only noise without any orientation error. However, the presence of high levels of noise masks the effect of sensor misorientations so that for SNRs lower than 5 the results become indistinguishable from those obtained in the presence of noise only (see Table 2). For deep sources, the amount of energy contained in horizontal components is small compared to that contained in the vertical components, and consequently the effect of sensor misorientations is decreased.

Velocity of the Medium

As VLP signals have typical wavelengths of tens to hundreds of kilometers, we have assumed throughout this study that local velocity perturbations do not have a significant effect on the propagating wavefronts and that a homogeneus medium is an appopriate representation of the first-order features of wave propagation. This, however, still leaves open the question of what an appropriate wave velocity is for the region within which the semblance method is to be applied. The selection of a velocity model relies on geologic and seismic information, which may or may not be accurate or

even available. In such cases, the velocity model used to calculate the travel times may not be the best representation of the medium.

To test the effects of medium velocity on the semblance locations, we use velocities of 3 and 5 km/sec, respectively, in an application to signals generated assuming a velocity of 4 km/sec (see the Synthetic Environment section). Our results suggest that the effects of velocity errors are small. This becomes clear when we examine how the semblance method works. The method evaluates the similarity between signals, shifted by the difference in travel times, and introduces a penalty function to account for the lack of rectilinearity in particle motions. The velocity of the medium only affects the travel times. If the travel-time differences are small compared to the period of the signal, the similarity between the shifted signals remains high within a large region around the source location, and therefore the semblance solution is most sensitive to the particle motion directions. In fact, the similarity among waveforms only plays a predominant role when the difference between arrival times at the furthest and nearest receivers represents a relatively large fraction of the dominant period. Figure 9 shows the maximum delays between arrivals at network receivers located furthest and nearest from the source, as a function of source position. The maximum delay ranges from 0.05 sec for deep sources located vertically beneath the network to 1 sec for surficial sources located outside the network. As our signals have dominant periods of 20 sec, an evaluation of semblance using the original definition (equation 2), which measures similarity among single-component waveforms aligned to correct for travel times, will not be sensitive to the source location. Furthermore, the maximum delays for deep sources located beneath the network are smaller than the 0.2-sec sampling interval of our synthetic signals. Thus the modifications of the method introduced by Kawakatsu *et al.* (2000) are mandatory to locate VLP signals. In this case, the semblance method basically turns into a procedure to quantify the crossing of the particle motion directions; hence velocity errors on the order of $\pm 25\%$ have little impact on the results.

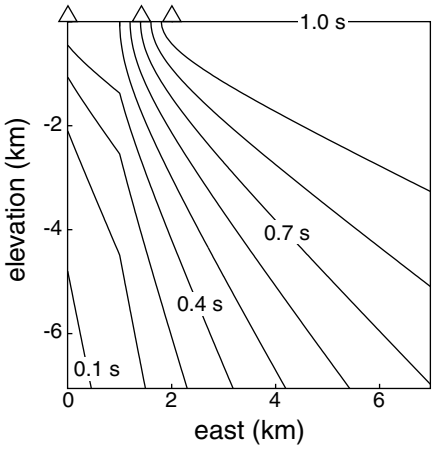

Figure 9. Contour plot of the differences between arrival times at network receivers located furthest from and nearest to the source as a function of source location.

Discussion

Definition of Error Limits in the Radial Semblance Method

In the past, the definition of an error region for source locations obtained by the semblance method has been made by selecting an arbitrary semblance level, for example 97% of the maximum semblance (Ohminato *et al.*, 1998; Chouet *et al.*, 1999). Note that due to the new scaling in the range [0 1] instead of [−1 1] in equation (9), this level translates here to ~98.5%. The numeric tests performed demonstrate that the selected level must account for the different effects considered and in particular for the amount of noise in the data. It seems obvious from our analyses that an appropriate definition of this semblance level may be $(1 - \delta S)S_{\max}$. In fact, we introduced δS to ensure that the real source lies in the region within which semblance is higher than that value.

Using the results in Table 2, we describe the functional dependence of δS on the SNR by a least-squares fit of δS to a power function of the SNR. The best fit yields

$$\delta S = 0.062\ \mathrm{SNR}^{-1.54}. \tag{16}$$

This equation can be applied to a particular data set to determine the level of semblance adequate to define the corresponding confidence regions. For example, the average SNR for the data analyzed by Chouet and Dawson (1997) is ~8, and they assumed a semblance level of 98.5% to define the size of the location error region. Equation (16) yields $\delta S = 0.25\%$, representing a level of 99.75% of the maximum semblance. This suggests that Chouet and Dawson (1997) were very conservative in the assessment of location errors.

Error regions may be assigned to particular source locations obtained from real data by following these steps: (1) apply the semblance method to the selected data, (2) determine the position $\vec{r}_{\max}$ and semblance value $S_{\max}$ of the maximum of the spatial semblance distribution, (3) evaluate the average SNR using equation (15), (4) determine δS using equation (16), and (5) find the region where semblance is larger than $(1 - \delta S)S_{\max}$. The source location and error region yielded by the semblance method are therefore given by

$$\begin{aligned} \vec{r} &= \vec{r}_{\max}, \\ \Delta\vec{r} &= \{\vec{r} | S(\vec{r}) \geq (1 - \delta S)S_{\max}\}. \end{aligned} \tag{17}$$

Validity of the Assumptions Underlying the Radial Semblance Method

In the previous sections, we have made assumptions about the source and medium to define a synthetic environ-

ment that enabled us to test the performance of the semblance method. The most critical assumption underlying the capabilities of the method is that the radiated wave field is dominated by radial motions. In our tests, we ensured the radial character of the signals by considering an isotropic source embedded in an infinite homogeneous elastic medium. Although this assumption is very restrictive, it has been readily met in many VLP volcanic signals observed so far (Neuberg *et al.*, 1994; Rowe *et al.*, 1998; Chouet *et al.*, 1999; Arciniega-Ceballos *et al.*, 1999; Hidayat *et al.*, 2000; Kawakatsu *et al.*, 2000; Almendros *et al.*, 2002a). For such signals, the radial semblance method constitutes a useful tool to obtain preliminary locations of the source of the VLP events. For some VLP signals, however, the assumption is too restrictive. These represent cases where source and/or path effects result in nonradial motions. These restrictive conditions are discussed in more detail in the following sections.

Free-Surface Effect. Particle motions produced by an isotropic source and recorded by a seismometer located at the surface of the Earth may not necessarily point to the source because of the effect of the free surface. The main effect of the free surface is a change in the apparent angle of incidence and azimuth of the waves produced by the impedance contrast between the solid and atmosphere. For a plane wave impinging a flat surface, well-known analytic formulas relating the actual and apparent incidence angles are available (e.g., problem 5.6 in Aki and Richards, 1980). However, the relationship between these angles in the more general situation of a free surface with topography is not straightforward (e.g, Ohminato and Chouet, 1997; Neuberg and Pointer, 2000; Chouet *et al.*, 2003).

We tested the effect of the free surface by generating synthetic seismograms for sources distributed at the grid nodes indicated by open circles in Figure 1. The synthetics were calculated by the discrete wavenumber method (Bouchon, 1979; Chouet, 1981; Herrman, 2002) assuming isotropic point sources embedded in a homogeneous elastic halfspace bounded by a flat free surface. We used *P*- and *S*-wave velocities of 4.0 and 2.5 km/sec, respectively, and considered parabolic-shaped source time functions with periods of 2, 8, and 20 sec. Figure 10 shows examples of synthetic particle motions calculated in this manner. For sources radiating signals with 2-sec periods (Fig. 10a) the particle motions do not intersect at a single point. Rather, they define a diffuse region shallower than the actual source. Although the size of this diffuse region decreases with increasing source depth (see rightmost panel in Fig. 10a), the depth of this region remains shallower than the actual source depth. For sources radiating VLP signals the situation improves considerably. For a source radiating a signal with period of 20 sec, the particle motions point back to the actual source location for all the distances considered (Fig. 10b). In that case the apparent and actual incidence angles are very similar and the source locations provided by the semblance method coincide with the actual source locations. These results suggest that VLP events with dominant periods in the range of a few tens of seconds can be reasonably well located by the semblance method provided the representation of the medium by a homogeneous half-space is adequate. For periods shorter than 10 sec, the accuracy of the semblance solution degrades and caution must be exercised in the interpretation of the results.

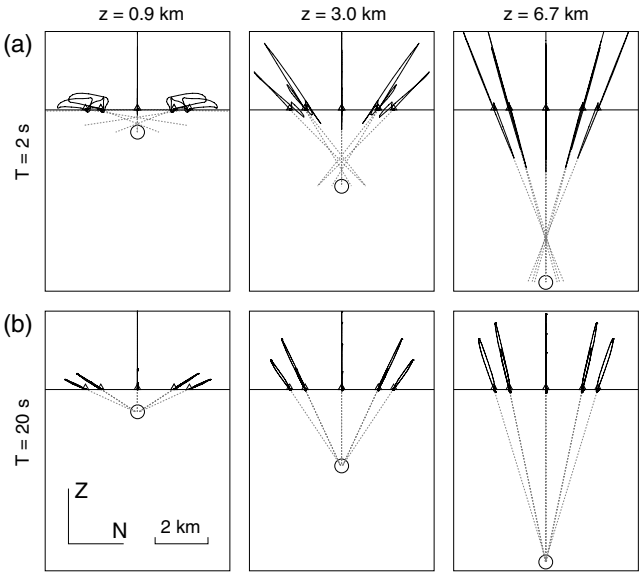

Figure 10. Effect of the free surface on particle motions. Solid lines are the particle motions including the effect of the free surface, projected in the north–south vertical plane, for sources located at $D = 1.0$, 3.4, and 7.7 km and $A = 30°$ (see Fig. 1). Dotted gray lines represent linear fits of the particle motion directions. The source position is marked by an open circle, and the source depth is indicated at the top of each panel. (a) The source time function has a dominant period of 2 sec (8-km wavelength). (b) The source time function has a dominant period of 20 sec (80-km wavelength).

Effect of Tilt. Contamination of the VLP signals by tilt results in the generation of apparent displacements due to rotation that are indistinguishable from the translation displacement field generated by a seismic source. Tilt effects are important mainly in the near field and strongly depend on the wavelenth of the signal and topography of the medium. Tilting may induce changes in the apparent directions of the observed particle motions, thereby introducing a bias in the source depth estimated by the radial semblance method.

We performed a series of tests to assess the importance of spurious displacements caused by tilting of the sensor. In these tests, synthetic seismograms were calculated by the finite-difference method (Ohminato and Chouet, 1997) for the topography of Kilauea Volcano, Hawaii. Details of the procedure can be found in Almendros *et al.* (2001a). Displacements and rotations were calculated separately for isotropic sources located at different depths under Kilauea Vol-

cano. We assumed a single-cycle cosine source time function with a period of 20 sec. Our results demonstrate that the apparent displacement produced by tilt only affects horizontal components at stations close to the source (at distances < 1 km) for shallow sources. Tilting was observed to degrade the rectilinearity of particle motions. However, it did not change the orientation of particle trajectories in a significant way. Based on these results, we conclude that tilt effects are trivial in the semblance solutions.

Nonradial Components in the Source Mechanism. In recent years, the source mechanisms of several VLP events have been determined by inversions of the waveforms recorded by broadband seismic networks (Ohminato *et al.*, 1998; Legrand *et al.*, 2000; Chouet *et al.*, 2003; Hidayat *et al.*, 2002; Kumagai *et al.*, 2003). These inversions suggest that VLP waveforms are consistent with source mechanisms representing volumetric changes of cracklike objects. In some cases, the VLP signals recorded in the near field of the source do not display rectilinear radial particle motions. Examples are the signals with periods near 10 sec recorded at Hachijo Island, Japan (Kumagai *et al.*, 2003), where the particle motions display elliptical orbits whose main axes do not always point to the source. The semblance method can not be applied in such cases. Additional observations of VLP volcanic events in the future may reveal further complexities in VLP signals not yet observed in the limited record of observations available at this time. Therefore, special care should be exercised when applying this method to signals displaying significant departure from radial rectilinearity to avoid meaningless results.

Conclusions

We have performed a study of the radial semblance method described by Kawakatsu *et al.* (2000) to test its capabilities and limitations. Applications of this method are justified and useful only when the source mechanisms produce mostly radial motions and the wavelengths are large enough so that path and free-surface effects can be neglected. Based on our analyses of the synthetic data described in this article, we conclude that the radial semblance method performs best when (1) the noise level is low enough to allow a good characterization of the waveforms (higher noise levels imply lower semblance values and larger location errors), (2) the sources are located at distances between one half of the average receiver spacing and about two times the network aperture, and (3) the orientations of the horizontal components of the seismometers are known at least within $\pm 10°$. When these conditions are met, the radial semblance method can provide relatively accurate source locations. The size of the error region depends mostly on the level of noise, and it can be estimated from the approximate formula given in equation (16). In general, a value of maximum semblance higher than ~ 0.7 should be a minimum requirement to trust any result from semblance analyses. Maximum values of semblance less than 0.7 may be caused by small SNRs, resulting in deviations from pure radial motions and waveform distortions. Another cause of small values of maximum semblance may be related to the presence of nonradial components in the particle motions associated with source and/or path effects. Topography may introduce strong distortions in the particle motions. This effect may be particularly significant in composite volcanoes characterized by steep slopes and complex three-dimensional velocity structures.

We conclude that the radial semblance method can provide an adequate tool to obtain fast, preliminary locations of VLP signals recorded by broadband networks. Refined source locations may then be determined by more elaborate methods based on waveform inversions, in which the effects of topography and velocity structure are fully accounted for.

Acknowledgments

We thank P. Dawson for his active involvement and support. S. Detweiler, P. Spudich, C. Rowe, and two anonymous reviewers contributed with useful comments. The work by J. Almendros was partially supported by projects REN2002-3833 of the Spanish Ministry for Science and Technology and EVR1-CT-2001-40021 of the European Union and by the research team RNM-104 of Junta de Andalucía, Spain.

References

Aki, K., and P. G. Richards (1980). *Quantitative Seismology*, W. H. Freeman, New York.

Almendros, J., B. Chouet, and P. Dawson (2001a). Spatial extent of a hydrothermal system at Kilauea Volcano, Hawaii, determined from array analyses of shallow long-period seismicity. I. Method, *J. Geophys. Res.* **106,** 13,565–13,580.

Almendros, J., B. Chouet, and P. Dawson (2001b). Spatial extent of a hydrothermal system at Kilauea Volcano, Hawaii, determined from array analyses of shallow long-period seismicity. II. Results, *J. Geophys. Res.* **106,** 13,581–13,597.

Almendros, J., B. Chouet, and P. Dawson (2002a). Identifying elements of the plumbing system beneath Kilauea volcano, Hawaii, from the source locations of very-long-period signals, *Geophys. J. Int.* **148,** 303–312.

Almendros, J., B. Chouet, P. Dawson, and C. Huber (2002b). Mapping the sources of the seismic wavefield at Kilauea Volcano, Hawaii, using data recorded on multiple seismic antennas, *Bull. Seism. Soc. Am.* **92,** 2333–2351.

Almendros, J., J. M. Ibáñez, G. Alguacil, and E. Del Pezzo (1999). Array analysis using a circular wave-front geometry: an application to locate the nearby seismo-volcanic source, *Geophys. J. Int.* **136,** 159–170.

Arciniega-Ceballos, A., B. Chouet, and P. Dawson (1999). Very-long-period signals associated with vulcanian explosions at Popocatepetl Volcano, Mexico, *Geophys. Res. Lett.* **26,** 3013–3016.

Aster, R., J. Lees, and J. Neuberg (Editors) (2000). "Broadband Seismic and Acoustic Observations of Volcanic Seismicity," *J. Volcanol. Geotherm. Res.* **101** (special issue).

Bouchon, M. (1979). Discrete wavenumber representation of elastic wave fields in three space dimensions, *J. Geophys. Res.* **85,** 3609–3614.

Chouet, B. (1981). Ground motion in the near field of a fluid-driven crack and its interpretation in the study of shallow volcanic tremor, *J. Geophys. Res.* **86,** 5985–6016.

Chouet, B. (1996). New methods and future trends in seismological volcano monitoring, in *Monitoring and Mitigation of Volcano Hazards*, R. Scarpa and R. Tilling (Editors), Springer, New York, 23–97.

Chouet, B., and P. Dawson (1997). Observations of very-long-period impulsive signals accompaying summit inflation at Kilauea volcano, Hawaii, in February 1997, (abstract), *EOS* **76,** no. 17, (Fall Meeting Suppl.), S11C-3.

Chouet, B., P. Dawson, T. Ohminato, M. Martini, G. Saccorotti, F. Giudicepietro, G. De Luca, G. Milana, and R. Scarpa (2003). Source mechanisms of explosions at Stromboli volcano determined from moment-tensor inversions of very-long-period data, *J. Geophys. Res.* **108,** 2019, doi 10.1029/2002JB001919.

Chouet, B., G. Saccorotti, M. Martini, P. Dawson, G. De Luca, G. Milana, and R. Scarpa (1997). Source and path effects in the wavefields of tremor and explosions at Stromboli volcano, Italy, *J. Geophys. Res.* **102,** 15,129–15,150.

Chouet, B., G. Saccorotti, P. Dawson, M. Martini, G. De Luca, G. Milana, and M. Cattaneo (1999). Broadband measurements of the sources of explosions at Stromboli volcano, Italy, *Geophys. Res. Lett.* **26,** 1937–1940.

Dawson, P., C. Dietel, B. Chouet, K. Honma, T. Ohminato, and P. Okubo (1998). A digitally telemetered broadband seismic network at Kilauea Volcano, Hawaii, *U.S. Geol. Surv. Open-File Rept. 98-108*, 122 pp.

Del Pezzo, E., J. M. Ibáñez, and M. La Rocca (1997). Observations of high-frequency scattered waves using dense arrays at Teide volcano, *Bull. Seism. Soc. Am.* **87,** 1637–1647.

Dreier, R., R. Widmer, R. Schick, and W. Zürn (1994). Stacking on broadband seismograms of shocks at Stromboli, *Acta Vulcanol.* **5,** 165–172.

Furumoto, M., T. Kunitomo, H. Inoue, and K. Yamaoka (1992). Seismic image of the volcanic tremor source at Iza-Oshima volcano, Japan, in *Volcanic Seismology*, P. Gasparini, R. Scarpa, and K. Aki (Editors), Springer, New York, 201–211.

Goldstein, P., and B. Chouet (1994). Array measurements and modeling of sources of shallow volcanic tremor at Kilauea Volcano, Hawaii, *J. Geophys. Res.* **99,** 2637–2652.

Herrmann, R. B. (2002). Computer Programs in Seismology, www.eas.slu.edu/People/RBHerrmann/ComputerPrograms.html, Saint Louis University (last accessed July 2003).

Hidayat, D., B. Chouet, B. Voight, P. Dawson, and A. Ratdomopurbo (2002). Source mechanism of very-long-period signals accompanying dome growth activity at Merapi volcano, Indonesia, *Geophys. Res. Lett.* **29,** 2118, doi 10.1029/2002GL015013.

Hidayat, D., B. Voight, C. Langston, A. Ratdomopurbo, and C. Ebeling (2000). Broadband seismic experiment at Merapi Volcano, Java, Indonesia: very-long-period pulses embedded in multiphase earthquakes, *J. Volcanol. Geotherm. Res.* **100,** 215–231.

Hill, D. P., P. Dawson, M. J. S. Johnston, A. M. Pitt, G. Biasi, and K. Smith (2002). Very-long-period volcanic earthquakes beneath Mammoth Mountain, California, *Geophys. Res. Lett.* **29,** 1370, doi 10.1029/2002GL014833.

Ito, A. (1985). High resolution relative hypocenters of similar earthquakes by cross-spectral analysis method, *J. Phys. Earth* **33,** 279–294.

Kaneshima, S., H. Kawakatsu, H. Matsubayashi, Y. Sudo, T. Tsutsui, T. Ohminato, H. Ito, K. Uhira, H. Yamasato, J. Oikawa, M. Takeo, and T. Iidaka (1996). Mechanism of phreatic eruptions at Aso volcano inferred from near-field broadband seismic observations, *Science* **273,** 642–645.

Kawakatsu, H., S. Kaneshima, H. Matsubayashi, T. Ohminato, Y. Sudo, T. Tsutsui, K. Uhira, H. Yamasato, H. Ito, and D. Legrand (2000). Aso94: Aso seismic observation with broadband instruments, *J. Volcanol. Geotherm. Res.* **101,** 129–154.

Kumagai, H., K. Miyakawa, H. Negishi, H. Inoue, K. Obara, and D. Svetsugu (2002). Magmatic dike resonances inferred from very-long-period seismic signals, *Science* **299,** 2058–2061.

Kumagai, H., T. Ohminato, M. Nakano, M. Ooi, A. Kubo, H. Inoue, and J. Oikawa (2001). Very-long-period seismic signals and caldera formation at Miyake Island, Japan, *Science* **293,** 687–690.

Legrand, D., S. Kaneshima, and H. Kawakatsu (2000). Moment tensor analysis of near field broadband waveforms observed at Aso volcano, Japan, *J. Volcanol. Geotherm. Res.* **101,** 155–169.

Linde, A., K. Agustsson, I. S. Sacks, and R. Stefansson (1993). Mechanism of the 1991 eruption of Hekla from continuous borehole strain monitoring, *Nature* **365,** 737–740.

McNutt, S. R. (1996). Seismic monitoring and eruption forecasting of volcanoes: a review of the state-of-the-art and case histories, in *Monitoring and Mitigation of Volcano Hazards*, R. Scarpa and R. Tilling (Editors), Springer, New York, 99–146.

Montalbetti, J. F., and E. R. Kanasewich (1970). Enhancement of teleseismic body phases with a polarization filter, *Geophys. J. R. Astr. Soc.* **21,** 119–129.

Neidel, N., and T. Tarner (1971). Semblance and other coherency measures for multichannel data, *Geophysics* **36,** 482–497.

Neuberg, J., and T. Pointer (2000). Effects of volcano topography on seismic broad-band waveforms, *Geophys. J. Int.* **143,** 239–248.

Neuberg, J., R. Luckett, M. Ripepe, and T. Braun (1994). Highlights from a seismic broadband array on Stromboli volcano, *Geophys. Res. Lett.* **21,** 749–752.

Nishimura, T., H. Nakamichi, S. Tanaka, M. Sato, T. Kobayashi, S. Ueki, H. Hamaguchi, M. Ohtake, and H. Sato (2000). Source process of very-long-period seismic events associated with the 1998 activity of Iwate Volcano, northeastern Japan, *J. Geophys. Res.* **105,** 19,135–19,147.

Ohminato, T., and B. Chouet (1997). A free surface boundary condition for including 3D topography in the finite-difference method, *Bull. Seism. Soc. Am.* **87,** 494–515.

Ohminato, T., B. Chouet, P. Dawson, and S. Kedar (1998). Waveform inversion of very-long-period impulsive signals associated with magmatic injection beneath Kilauea Volcano, Hawaii, *J. Geophys. Res.* **103,** 23,839–23,862.

Poupinet, G., A. Ratdomopurbo, and O. Coutant (1996). On the use of earthquake multiplets to study fractures and the temporal evolution of an active volcano, *Ann. Geofis.* **39,** 253–264.

Rowe, C. A., R. C. Aster, P. R. Kyle, J. W. Schlue, and R. R. Dibble (1998). Broadband recording of Strombolian explosions and associated very-long-period seismic signals on Mount Erebus volcano, Ross Island, Antarctica, *Geophys. Res. Lett.* **25,** 2297–2300.

Saccorotti, G., B. Chouet, and P. Dawson (2001). Wavefield properties of a shallow long-period event and tremor at Kilauea Volcano, Hawaii, *J. Volcanol. Geotherm. Res.* **109,** 163–189.

Uhira, K., and M. Takeo (1994). The source of explosive eruptions of Sakurajima volcano, Japan, *J. Geophys. Res.* **99,** 17,775–17,789.

Instituto Andaluz de Geofísica
Universidad de Granada
Granada, Spain
(J.A.)

U.S. Geological Survey
Menlo Park, California
(B.C.)

Manuscript received 25 June 2002.